Electronic Supplementary Material (ESI) for Physical Chemistry Chemical Physics.

Supplementary Information

Structure of Water-in-Salt and Water-in-Bisalt Electrolytes

Miguel Angel González, Hiroshi Akiba, Oleg Borodin, Gabriel Julio Cuello, Louis Hennet, Shinji Kohara, Edward J. Maginn, Lucile Mangin-Thro, Osamu Yamamuro, Yong Zhang, David L. Price and Marie-Louise Saboungi.

Table S1. Concentrations (c), atomic numbers (Z), and coherent neutron scattering lengths (b_{coh}) for the 13.9 m LiTFSI solution. Neutron scattering lengths from [1].

Element	**c**	**Z**	**b_{coh}**	**c × Z**	**c × b_{coh}**
Li	0.036	3	–1.9	0.107	–0.068
C (TFSI)	0.071	6	6.646	0.429	0.475
N (TFSI)	0.036	7	9.36	0.250	0.334
O (TFSI)	0.143	8	5.803	1.143	0.829
F (TFSI)	0.214	9	5.654	1.929	1.212
S (TFSI)	0.071	16	2.847	1.143	0.203
O (water)	0.143	8	5.803	1.143	0.800
H (water)	0.286	1	–3.739	0.286	–1.068
D (water)	0.286	1	6.671	0.286	1.906

Table S2. Concentrations (c), atomic numbers (Z), and coherent neutron scattering lengths (b_{coh}) for the 21 m LiTFSI solution. Neutron scattering lengths from [1].

Element	**c**	**Z**	**b_{coh}**	**c × Z**	**c × b_{coh}**
Li	0.042	3	–1.9	0.125	–0.079
C (TFSI)	0.083	6	6.646	0.500	0.554
N (TFSI)	0.042	7	9.36	0.292	0.390
O (TFSI)	0.167	8	5.803	1.333	0.967
F (TFSI)	0.250	9	5.654	2.250	1.413
S (TFSI)	0.083	16	2.847	1.333	0.237
O (water)	0.111	8	5.803	0.889	0.645
H (water)	0.222	1	–3.739	0.222	–0.831
D (water)	0.222	1	6.671	0.222	1.482

Table S3. Concentrations (c), atomic numbers (Z), and coherent neutron scattering lengths (b_{coh}) for the (21 m + 7 m) LiTFSI-LiOTf solution. Neutron scattering lengths from [1].

Element	**c**	**Z**	**b_{coh} (fm)**	**c × Z**	**c × b_{coh}**
Li	0.049	3	–1.9	0.148	–0.094
C (TFSI)	0.074	6	6.646	0.444	0.492
N (TFSI)	0.037	7	9.36	0.259	0.347
O (TFSI)	0.148	8	5.803	1.185	0.860
F (TFSI)	0.222	9	5.654	2.000	1.256
S (TFSI)	0.074	16	2.847	1.185	0.211
C (OTf)	0.012	6	6.646	0.074	0.082
O (OTf)	0.037	8	5.803	0.296	0.215
F (OTf)	0.037	9	5.654	0.333	0.209
S (OTf)	0.012	16	2.847	0.198	0.038
O (water)	0.099	8	5.803	0.790	0.573
H (water)	0.198	1	–3.739	0.198	–0.739
D (water)	0.198	1	6.671	0.198	1.318

Table S4. Composition of MD simulation boxes and corresponding densities at 298 K. Density values given in parentheses correspond to the experimental densities at 298 K estimated with the equation and parameters given in [2]. Two polarizable force field versions were used: f1p from previous work [3] and f1w modified in this work (referred to as Pol1 and Pol2 in the figures in the main paper).

LiTFSI molality (m) [force field]	Number of LiTFSI	Number of water	Density (g/cm^3)
Polarizable MD using the original (f1p) and modified (f1w) versions of APPLE&P force fields			
13.9 [f1p]	192	768	1.580 (1.647)
21 [f1p]	192	512	1.650 (1.714)
21 [f1w]	384	1024	1.725 (1.714)
21 +7 [f1p]	192 TFSI / 64 LiOTf	512	1.666
Non-polarizable MD			
13.9	626	2500	1.646 (1.647)
20	720	2000	1.719 (1.708)

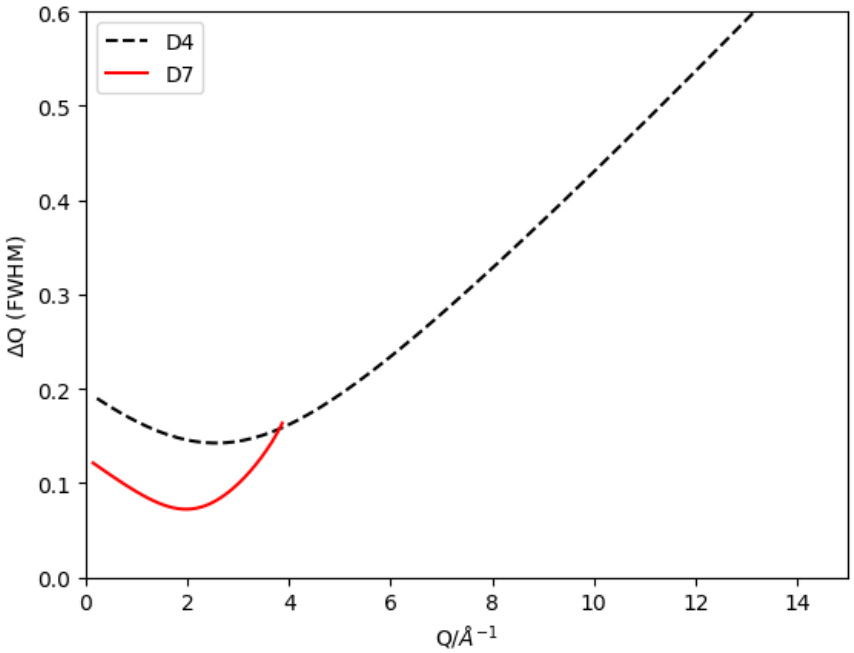

Figure S1. Instrumental resolution of D4 and D7, calculated using the formula of Caglioti *et al.* [4] with parameters U = 7.99, V = –7.75 and W = 3.2 for D7 [5] and U = 9.3805, V = –1.9033 and W = 0.2029 for D4 [6].

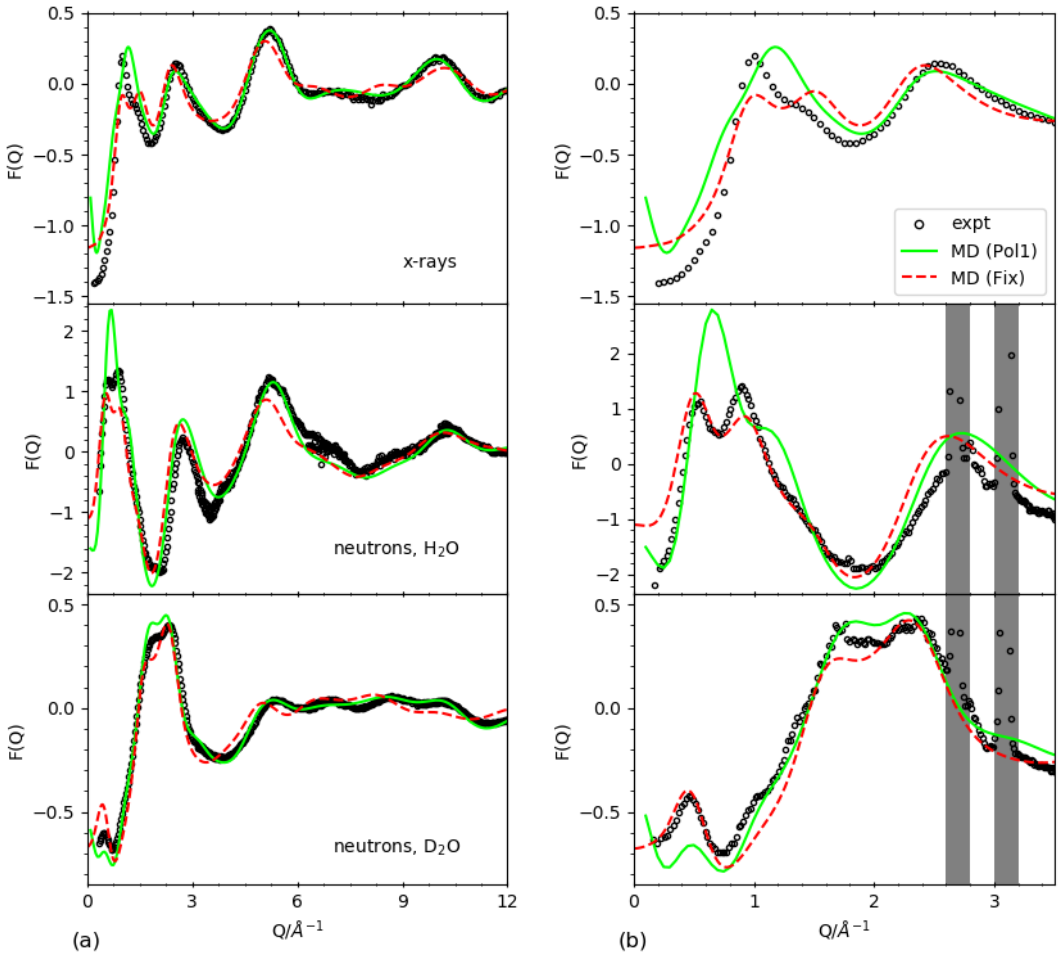

Figure S2. Comparison of the experimental $F(Q)$ for the 13.9 m solution derived from HEXRD measurements at SPring-8 (top panels), neutron diffraction on H_2O solutions (middle panels), and neutron diffraction on D_2O solutions (bottom panels) with those calculated from the polarizable (continuous line) and non-polarizable (dashed line) simulations. Left: full Q range showing the more relevant features; for simplicity, in the middle and bottom panels only the experimental results obtained on D4 are shown; in both panels, the plotted MD curves have been smeared by the instrument resolution. Right: blow-up showing the low-Q region where the main differences between experiment and simulation are observed; here only data from D7 are shown in the middle and bottom panels, and no smearing is applied to the MD curves.

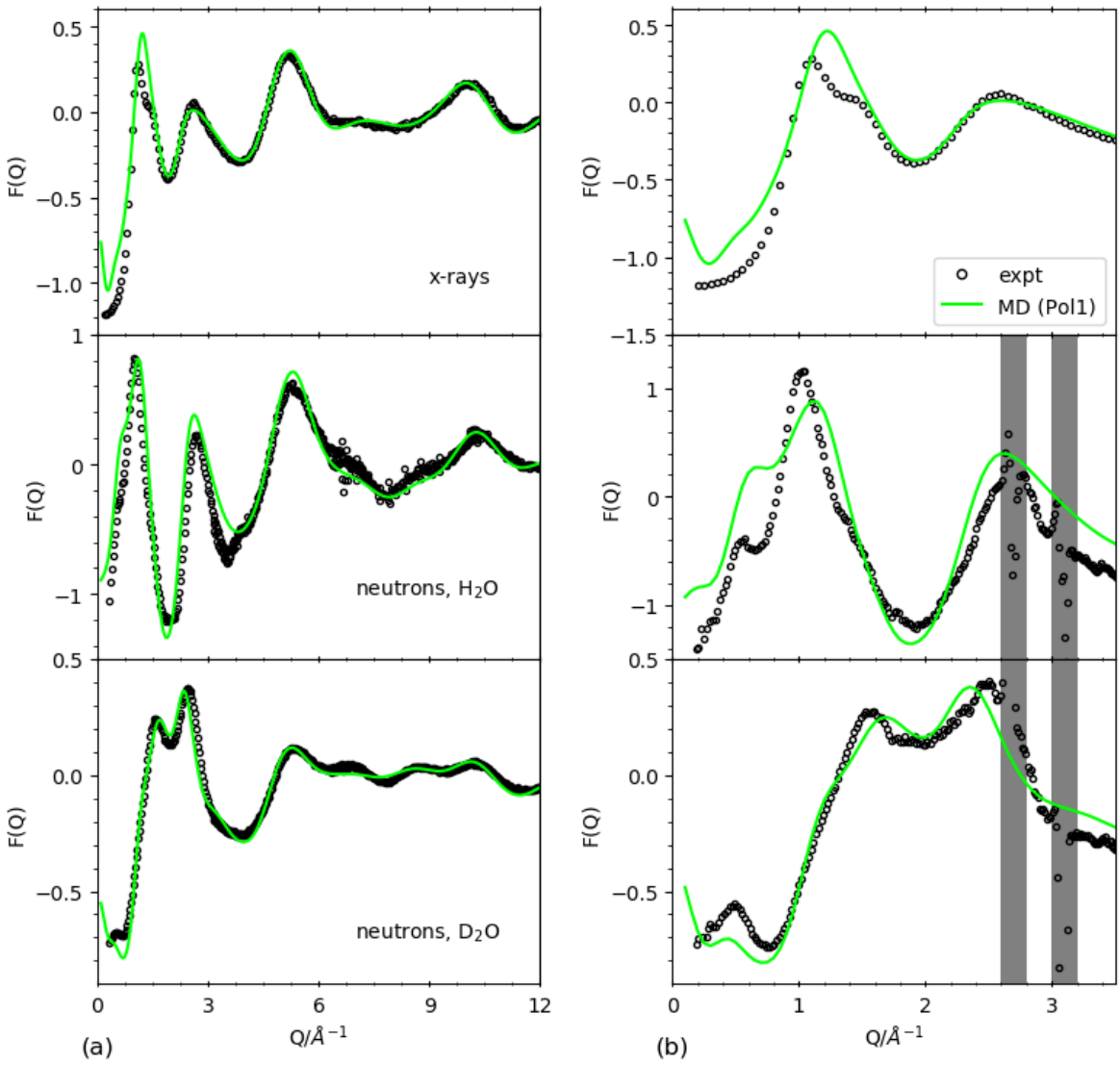

Figure S3. Comparison of the experimental $F(Q)$ for the (21 m + 7 m) solution derived from HEXRD measurements at SPring-8 (top panels), neutron diffraction on H_2O solutions (middle panels), and neutron diffraction on D_2O solutions (bottom panels) with those calculated from the polarizable simulations. Left: full Q range showing the more relevant features; for simplicity, in the middle and bottom panels only the experimental results obtained on D4 are shown; in both panels, the plotted MD curves have been smeared by the instrument resolution. Right: blow-up showing the low-Q region where the main difference between experiment and simulation are observed; here only data from D7 are shown in the middle and bottom panels, and no smearing is applied to the MD curves.

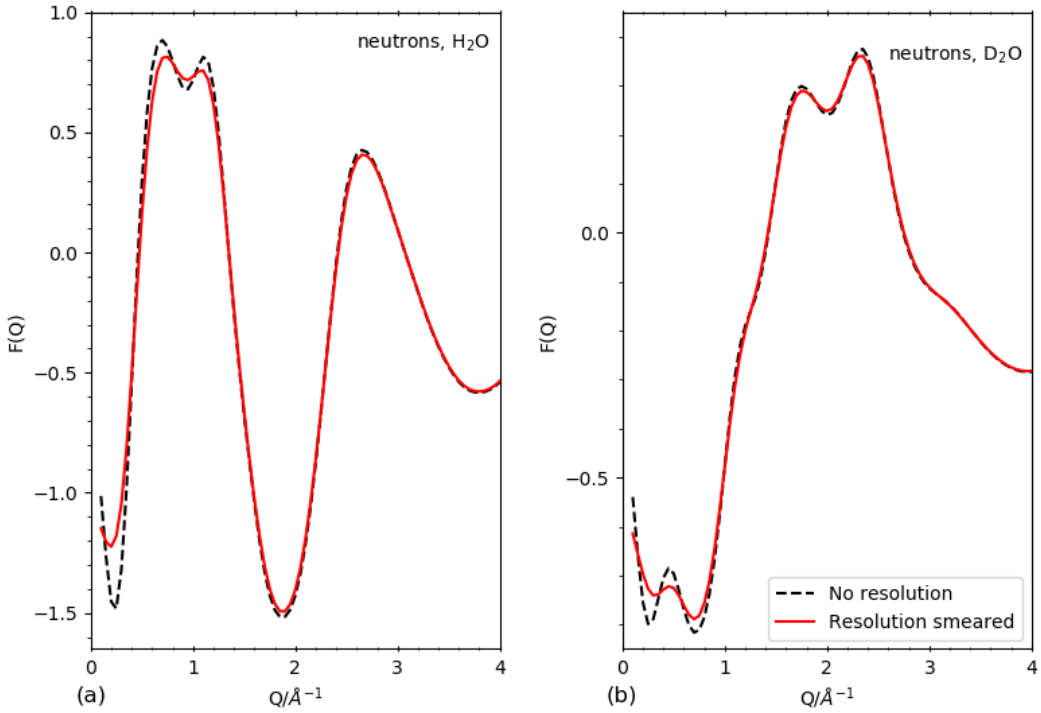

Figure S4. $F(Q)$ from the polarizable simulations for the (left) H_2O and (right) D_2O 21m solutions, showing the effect of applying a resolution smearing equivalent to the instrumental resolution of D4. We used a Gaussian resolution function with a Q-dependent FWHM given by the D4 line shown in Fig. S1.

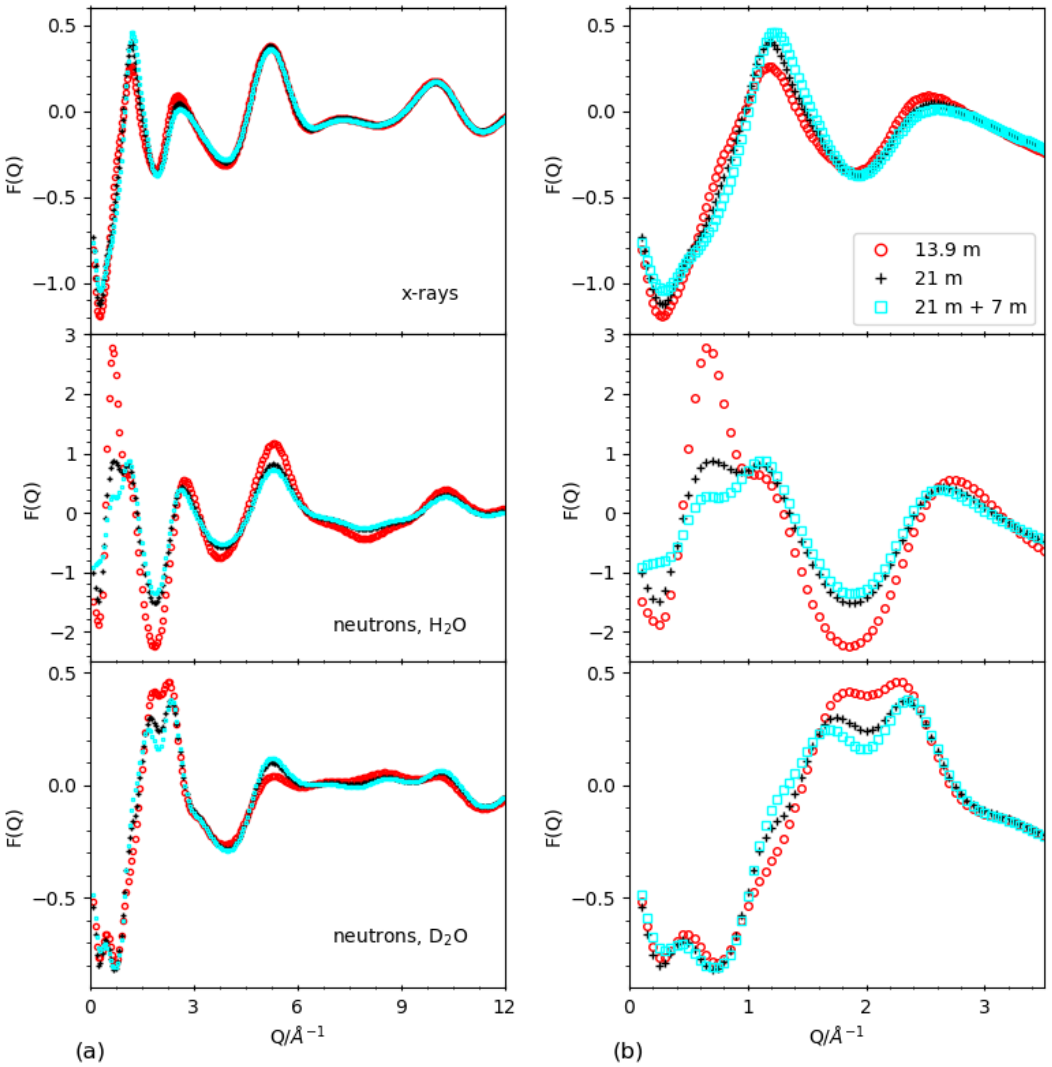

Figure S5. $F(Q)$ for the 13.9 m, 21 m and (21 m + 7 m) solutions derived from the polarizable MD simulations using x-ray weights (top panels) and neutron weights for H_2O (middle panels) and D_2O solutions (bottom panels). Left: full Q range showing the more relevant features. Right: blow-up of the low-Q region showing the main changes in $F(Q)$ with increasing salt concentration.

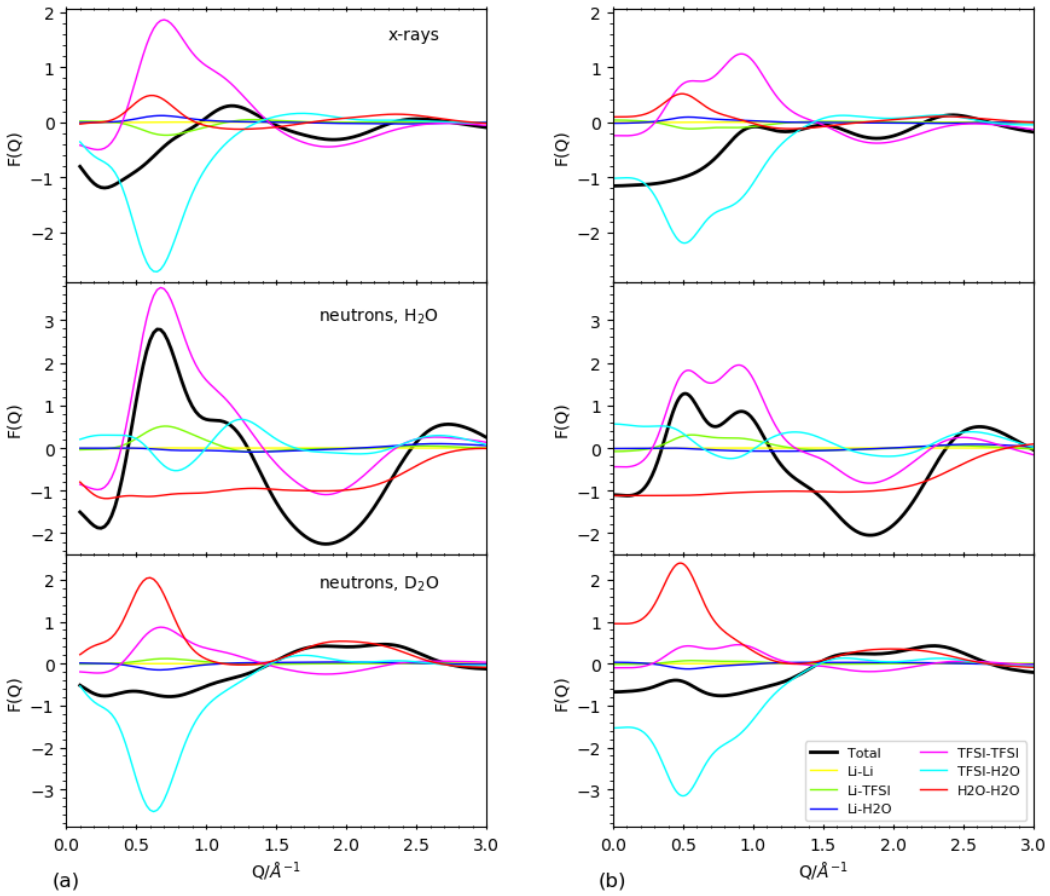

Figure S6. Contributions to the x-ray (top panels) and neutron weighted structure factors for H_2O (middle panels) and D_2O (bottom panels) for different molecular/ionic pairs (see text), showing the respective contribution of each partial to the MD weighted average *F(Q)*s of the 13.9 m solution shown in Fig. S2 and replotted here as the solid thick line. Results from the (left) polarizable (Pol1) and (right) non-polarizable simulations (Fix).

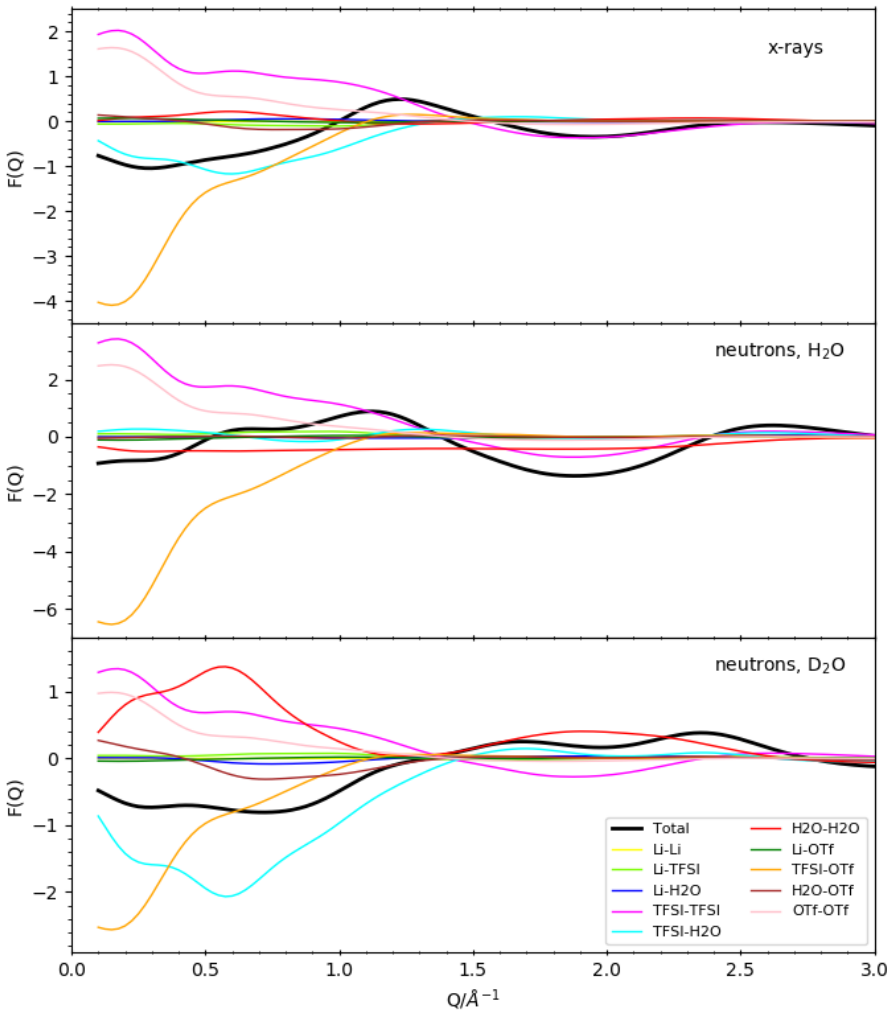

Figure S7. Contributions to the x-ray (top panels) and neutron weighted structure factors for H_2O (middle panels) and D_2O (bottom panels) for different molecular/ionic pairs (see text of main paper), showing the respective contribution of each partial to the MD weighted average *F(Q)*s of the (21 m + 7 m) solution from the polarizable simulations shown in Fig. S3 and replotted here as solid thick lines.

.

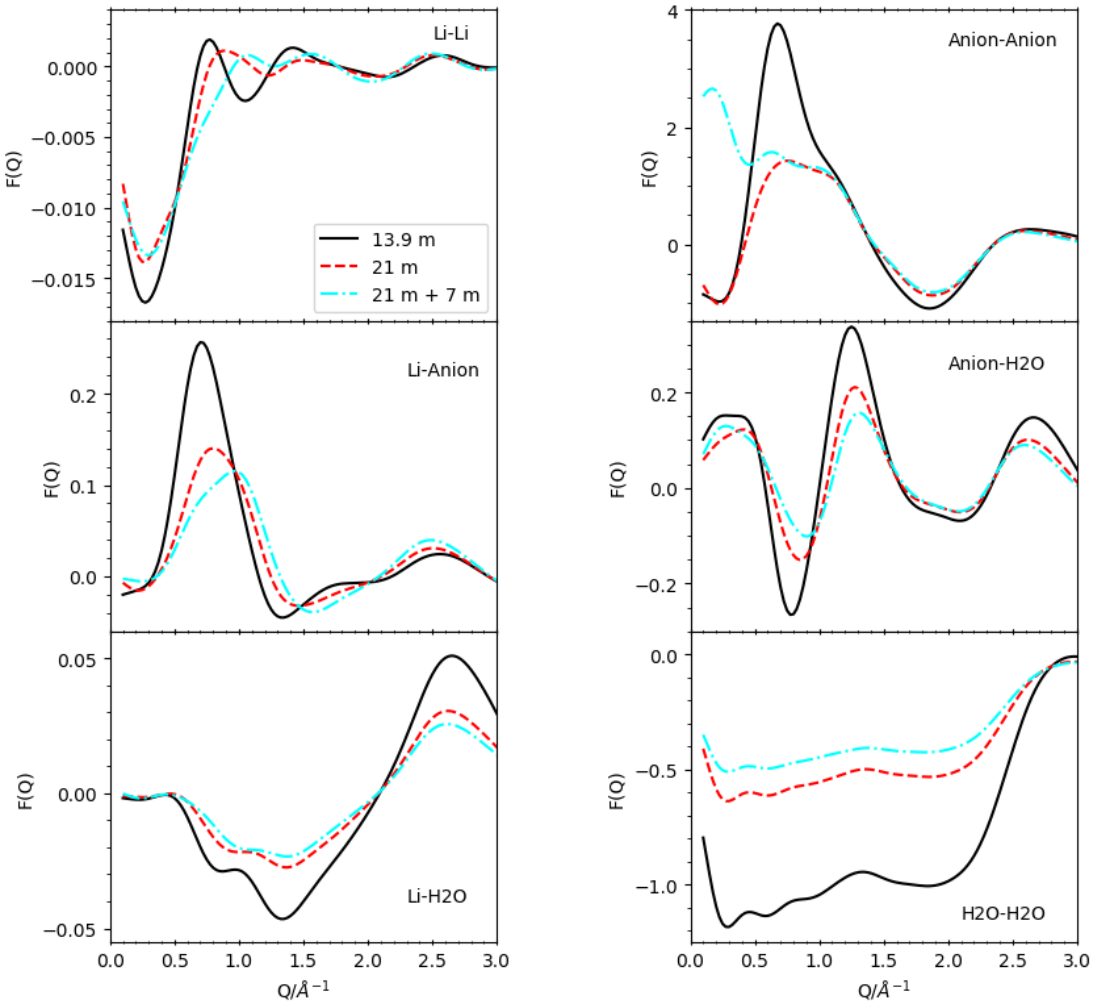

Figure S8. Contributions to the neutron weighted structure factors for H_2O solutions for different molecular/ionic pairs as a function of the concentration (see text), grouping together the two anions for the (21 m + 7 m) solution, obtained from the polarizable simulations.

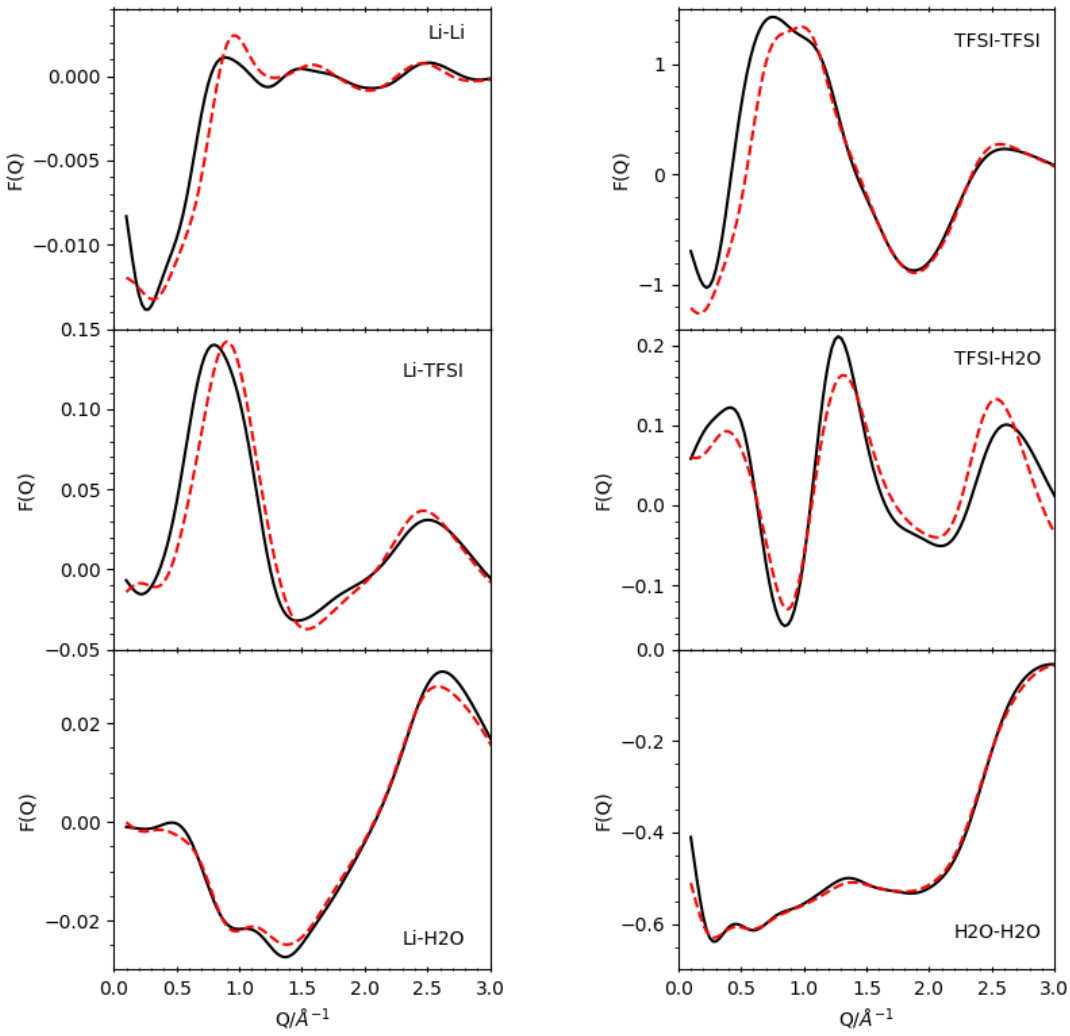

Figure S9. The six grouped molecular/ionic partial interference functions obtained from the polarizable simulations for the 21 m H_2O solution with the original (continuous black line) and modified (dashed red line) force fields.

APPLE&P Polarizable Force Field Revision

One source of inaccuracy of the solution structural description by the APPLE&P force field could be due to an inadequate description of water near the -CF_3 part of the $TFSI^-$ anions. We selected a small model system of C_2F_6/H_2O that allows an accurate prediction of binding energy using quantum chemistry methods in order to benchmark the ability of the force field to describe this interaction. A coupled cluster method with iterative inclusion of single and double excitations with perturbative inclusion of triple excitations (CCSD(T)) was used together with the basis set (CSB) extrapolation. Such CCSD(T)/CBS energy is a reliable benchmark for testing ability of APPLE&P force field to predict binding energies. The CCSD(T)/CBS extrapolated energy was estimated from MP2/CBS energy by adding a difference (CCSD(T)/aug-cc-pvTz – MP2/aug-cc-pvTz). The MP2/CBS energy was extrapolated using $E(CBS)=a/(X^3)+c$ relation, where X=3 for aug-cc-pvTz and X=4 for aug-cc-pvQz, while a,c are constants determined by fitting binding energies from MP2/aug-cc-pvQz and MP2/aug-cc-pvTz calculations. The resulting raw and basis set superposition error (BSSE) corrected energies are listed in Table S5 corresponding to the C_2F_6/H_2O geometries optimized at the MP2/aug-cc-pvTz level and shown in Figure S10.

The previously used force field (FF, f1p) predicts lower binding energies of water to C_2F_6 compared to CCSD(T)/CSB QC values. The repulsion parameters of the exp-6 non-bonded terms were modified in this work (FF, f1w) to bring the C_2F_6/H_2O binding energies in better agreement with QC values. The C_m-Ow repulsion-dispersion parameters from PEO-H_2O force field were adopted from [7]. Weaker repulsion between -CF_3 groups and H_2O results in a slight increase of electrolyte density as shown in Table S4. Force field files with the original (ff.dat_f1p_C2F6-H2O) and revised (ff.dat_f1w_C2F6-H2O) parameters are included in the tar archive provided together with the SI.

Table S5. The non-bonded component of the binding energies (in kcal mol^{-1}) for C_2F_6/H_2O at MP2/aug-cc-pvTz geometries shown in Figure S10.

	geometry (a)		**geometry (b)**		**geometry (c)**	
		BSSE		BSSE		BSSE
method	raw	corrected	raw	corrected	raw	corrected
MP2/aug-cc-pvTz	-1.11	-0.62	-1.33	-0.90	-1.51	-1.07
MP2/aug-cc-pvQz	-0.91	-0.67	-1.18	-0.96	-1.35	-1.14
MP2/CBS	-0.76	-0.71	-1.07	-1.00	-1.23	-1.19
CCSD(T)/aug-cc-pvTz	-1.30	-0.79	-1.50	-1.05	-1.71	-1.26
CCSD(T)/CBS	**-0.95**	**-0.88**	**-1.24**	**-1.15**	**-1.43**	**-1.38**
FF (f1w, revised)		-0.84		-1.29		-0.93
FF (f1p)		-0.49		-1.07		-0.76

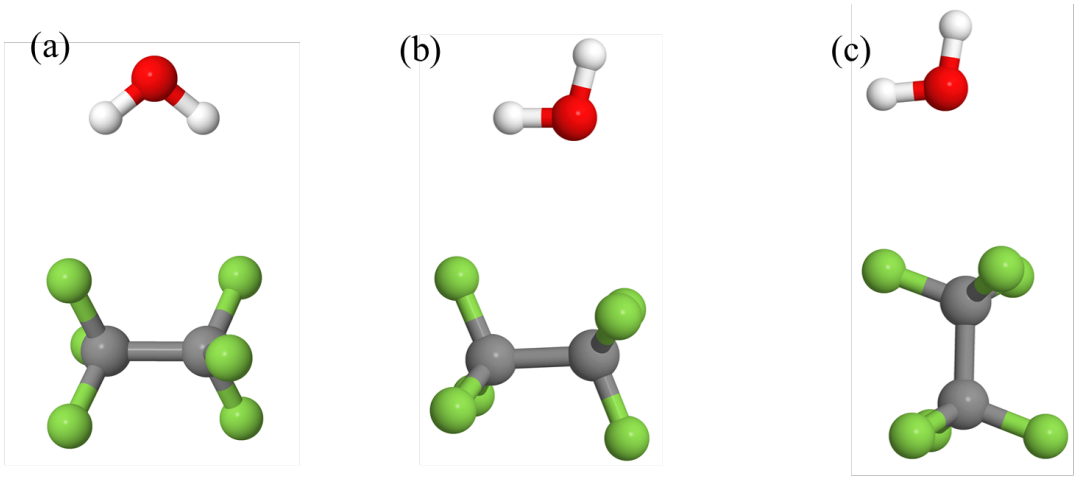

Figure S10. The C_2F_6/H_2O geometries optimized at MP2/aug-cc-pvTz level. The basis set superposition error (BSSE) corrected CCSD(T)/(complete basis set extrapolation, CBS) non-bonded part of the binding energy is shown in kcal mol^{-1} together with the energies obtaining using force fields (FFs).

Summary of the Polarized MD Simulation Methodology using APPLE&P

The Ewald summation method was used for the electrostatic interactions between permanent charges with permanent charges and permanent charges with induced dipole moments with $k = 7^3$ vectors. Multiple timestep integration was employed with an inner timestep of 0.5 fs (bonded interactions); a central time step of 1.5 fs for all nonbonded interactions within a truncation distance of 7.0-9.0 Å and an outer timestep of 3.0 fs for all nonbonded interactions between 7.0 Å and the nonbonded truncation distance of the smaller of 14-16 Å. The reciprocal part of the Ewald summation was updated only at the largest of the multiple time steps. A Nose-Hoover thermostat and a barostat were used to control the temperature and pressure with associated frequencies of 10^{-2} and 0.5×10^{-3} fs. The atomic coordinates were saved every 2 ps for post-analysis. MD simulations runs were 70 ns for 13.9 m, 227 ns for 21 m using f1p force field and 24.7 ns for f1w force field for 21 m.

Convergence of the simulated density in the non-polarized NPT

As shown in Fig. S11, the simulated density converged within 1 ns and the 1-2 ns simulation was used to calculate the equilibrium density.

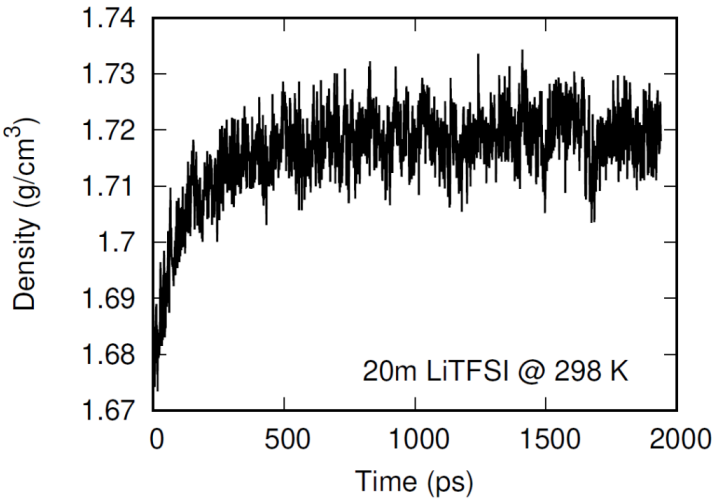

Figure S11. Time evolution of the density on the non-polarized NPT simulation for the 20 m LiTFSI-H_2O solution at 298 K.

References

[1] V. F. Sears. Neutron scattering lengths and cross sections. *Neutron News,* 1992*,* **3**, 26-37.

[2] W. J. R. Gilbert, J. Safarov, D. L. Minnick, M. A. Rocha, E. P. Hassel, and M. B. Shiflett. Density, viscosity, and vapor pressure measurements of water + lithium bis(trifluoromethylsulfonyl)imide solutions. *J. Chem. Eng. Data,* 2017, **62**, 2056-2066.

[3] O. Borodin, L. Suo, M. Gobet, X. Ren, F. Wang, A. Faraone, J. Peng, M. Olguin, M. Schroeder, M. S. Ding, E. Gobrogge, A. von Wald Cresce, S. Munoz, J. A. Dura, S. Greenbaum, C. Wang and K. Xu, Liquid Structure with Nano-Heterogeneity Promotes Cationic Transport in Concentrated Electrolytes, *ACS Nano*, 2017, **11**, 10462-10471.

[4] G. Caglioti, A. Paoletti, and F. P. Ricci. Choice of collimators for a crystal spectrometer for neutron diffraction. *Nuclear Instrum,* 1958*,* **3**, 223-228.

[5] T. Fennell, L. Mangin-Thro, H. Mutka, G. J. Nielsen, and A. R. Wildes. Wavevector and energy resolution of the polarized diffuse scattering spectrometer D7. *Nuclear Instrum. Methods Phys. Res. A,* 2017, **857**, 24-30.

[6] H. E. Fischer. D4c resolution of the standard configuration (0.5 Å wavelength, Cu220 monochromator, 5 mm diameter sample). *Private communication*.

[7] O. N. Starovoytov, O. Borodin, D. Bedrov and G. D. Smith, Development of a Polarizable Force Field for Molecular Dynamics Simulations of Poly (Ethylene Oxide) in Aqueous Solution, *J. Chem. Theory Comput.*, 2011, **7**, 1902-1915.